Journal of Solar Energy Research (JSER)

Journal homepage: www.jser.ut.ac.ir

Parametric Optimization of PEM Electrolyzer Integrated with Solar Multi-Generation System Based On Exergy, Cost and Environmental Criteria

S.Nazer, F.Ahmadi Boyaghchi*

*Depatement of Mechanical Engineering, Faculty of Engineering and Technology, Alzahra University, Tehran, Iran. *E-mail: fahmadi@alzahra.ac.ir*

ARTICLE INFO

Received: 12 May 2016
Received in revised form: 10 July 2016
Accepted: 15 July 2016
Available online: 17 July 2016

Keywords:
solar energy; hydrogen production;exergoeconomic; exergoenvironment

A B S T R A C T

A theoretical investigation is conducted for a novel renewable energy based multigeneration system producing hydrogen by means of a proton exchange membrane (PEM) electrolyzer as well as several commodities, namely power, drying, cooling and hot water. Engineering Equation Solver (EES) software is applied to model the PEM electrolyzer and multigeneration system. Thermodynamic, cost and environmental impact evaluations are included for hydrogen produced by considering the major design parameters. Outcomes indicate that the turbine inlet press. increases the hydrogen exergy efficiency of the system within 56% and decreases its environmental impact by about 3.8 % whereas it has a negative effect on the hydrogen cost produced. Moreover, the current density and temperat. of the electrolyzer affect the cost and environmental impact of hydrogen negatively.

1. Introduction

Hydrogen (H2) has various applications in industry. The largest application of H2 is for the processing of fossil fuels, and in the production of ammonia. It is used as a hydrogenating agent, particularly in increasing the level of saturation of unsaturated fats and oils (found in items such as margarine), and in the production of methanol. It is similarly the source of hydrogen in the manufact. of hydrochloric acid. H2 is also used as a reducing agent of metallic ores [1]. Apart from its use as a reactant, H2 has wide applications in physics and engineering. It is used as a shielding gas in welding methods such as atomic hydrogen welding [2]. H2 is used as the rotor coolant in electrical generators at power stations, because it has the highest thermal conductivity of any gas. Liquid H2 is also used in cryogenic research, including super conductivity studies [3]. In more recent applications, H2 is used p. or mixed with nitrogen (sometimes called forming gas) as a tracer gas for minute leak detection. Applications can be found in the automotive, chemical, power generation, aerospace, and telecommunications industries [4]. Hydrogen is an authorized food additive that allows food package leak testing among other anti-oxidizing properties. Hydrogen can be produced in a relatively environmentally benign manner (depending on the source of the input energy) via splitting water by photocatalysis, thermochemical cycles and electrolysis. Currently, both thermochemical and photocatalysis hydrogen production are not economically competitive. Water electrolysis is a mat. technology for large scale hydrogen production. Hydrogen production by proton exchange membrane (PEM) electrolysis has numerous advantages, such as low environmental impact and easy maintenance [5]. Recently, several investigation have been carried out on H2 production using the multigeneration energy systems owing to their high thermodynamic performances. Ozturk and Dincer [6] developed a new multi-generation system for solar-based hydrogen production. Thermodynamic analysis of the proposed system which produces a number of outputs, such as power, heating, cooling, hot water, hydrogen and oxygen was conducted. Several parametric studies were performed

in order to examine the effects of varying operating conditions on the exergy efficiencies of the sub-systems as well as the whole system. The solar-based multigeneration system which had an exergy efficiency of 57.35%, was obtained to be higher than using these sub-systems separately. Increasing the reference temperat. affected the exergy efficiency of the Rankine, organic Rankine, hydrogen production and utilization cycles as well as the multi-generation system positively. Ahmadi et al. [7] proposed and thermodynamically assessed a new multi-generation system based on a biomass combustor, an organic Rankine cycle, an absorption chiller (LiBr-water) and a proton exchange membrane (PEM) electrolyzer to produce hydrogen, and a domestic water heater for hot water production. A parametric study was performed to investigate the effects of several important design parameters on the energy and exergy efficiencies of the system. Ahmadi et al. [8] reported a comprehensive thermodynamic modeling and multi-objective optimization of a multigeneration energy system, based on a micro gas turbine, a dual press. heat recovery steam generator, an absorption chiller, an ejector refrigeration cycle, a domestic water heater and a PEM electrolyzer, that produced multiple commodities: power, heating, cooling, hot water and hydrogen. Energy and exergy analyses and an environmental impact assessment were included. They [9] also developed a new multigeneration system based on an ocean thermal energy conversion system and equipped with flat plate and photovoltaic/thermal (PV/T) collectors, a reverse osmosis desalination unit to produce fresh water, a single effect absorption chiller (LiBr-Water) and a PEM electrolyzer. Energy and exergy analyses were employed to determine the irreversibilities in each component and assess system performance. A multi-objective optimization method based on a fast and elitist non-dominated sorting genetic algorithm (NSGA-II) was applied to determine the best design parameters for the system. Bicer and Dincer [10] developed a new combined system, using solar and geothermal resources, for hydrogen production, along with power generation, cooling and heating, was proposed and analyzed for practical applications. This combined renewable energy system consisted of solar PV/T modules for heating, water heating and hydrogen production purposes and geothermal energy for electricity, cooling and hydrogen production. Energy and exergy analyses were conducted to assess the performance of the cycle, and the effects of various system parameters on energy and exergy efficiencies of the overall system and its subsystems were also studied.

In this communication, a novel solar-geothermal multigeneration system equipped with a PEM electrolyzer to produce hydrogen is proposed and assessed using thermodynamic, cost and EI concepts. The following objective of this research are performed:

(I) Modelling the proposed renewable system.

(II) Validating the PEM electrolyzer with experimental data.

(III) Conducting the cost and EI rate of the overall system.

(IV) Evaluating the effects of design parameters on thermodynamic, cost and EI of PEM electrolyzer.

2. Materials and Methods

2.1. System description

Fig. 1 illustrates the schematic of the multi-generation energy system proposed. Isobotane is selected as a convenient working fluid inside ORC. The desire working fluid is superheated by receiving heat from the hot brine (145oC and 2600 kPa) when passes through heat exchanger 1. Then, it is expanded inside the turbine to produce power (838.5 kW) and discharged to the condenser to reject heat to the water (15oC). The saturated working fluid leaving the condenser enters the pump 2 to complete the cycle. A portion of warm water inside the condenser is used to provide the heating load for the domestic application and the remaining flows into the PEM electrolyzer. In PEM electrolyzer, the warm water is split into the H2 and O2 by the electricity generated via CPVT. CPVT is cooled by water and its heat is rejected to the required air for drying in heat exchanger 2. At point 26, the warm air (85oC) follows into the dryer to reduce the relative moist. of the date from 60% to 20% flowing with flow rate of 2.1 kg/s. On the other hand, in the magnetic refrigerator, R134a leaving heat exchanger 3 enters the cooler magnetocaleric bed to cool up to 0oC and provide the cooling load inside the evaporator. The warm R134a passes through the heater magnetocaleric bed and preheats the drying air up to 39oC. The saturated liquid flows into pump 3 to make up the press. loss inside the magnetic refrigeration cycle.

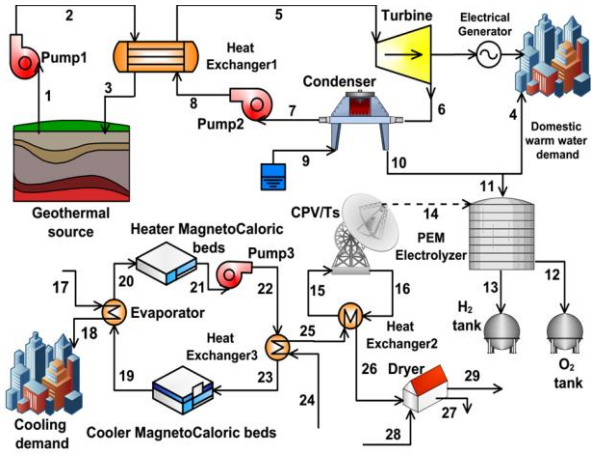

Figure 1. Schematic diagram of proposed system

To simplify the simulation of the proposed system, several assumption are considered as follows [5] and [11]:

- The temperat. and press. of the dead state are considered as 15oC and 101.325 kPa,

respectively.

- All components operate under the steady state condition.
- The kinetic and potential energyies and exergies are considered negligible.
- The reactants and products during the chemical reactions have the press. of 101.325 kPa.
- The outlet flow of the condenser is in the liquid saturation state.
- The isentropic efficiencies of the pump and turbine are 80% and 85%, respectively
- All components of the desired system are considered control valume.
- The system is assumed to be located at Bandar-Abbas with latitude and longitude of 56.38oN and 27.22oE, respectively with the average monthly irradiation of 0.6644 GJ/m2.

2.2. Mass and energy balances

By considering the assumption made, mass and energy relations are applied for each component as follows [12]:

$$\sum \dot{m}_i = \sum \dot{m}_e \quad (1)$$

$$\dot{Q} + \sum_i \dot{m}h = \dot{W} + \sum_e \dot{m}h \quad (2)$$

Here, and indicate the heat and work rate, respectively. and h represent the mass flow rate and specific enthalpy.

2.3. Exergy balance

The total exergy destruction rate ($\dot{E}x_d$) for the kth component can be determined with fuel exergy ($\dot{E}x_d$) and product exergy ($\dot{E}x_d$) as follows [5]:

$$\dot{E}x_{d,k} = \dot{E}x_{F,k} - \dot{E}x_{P,k} \quad (3)$$

The exergy efficiency of each component can be expressed as the ratio of the product exergy output rate to the exergy input (fuel) rate as follows [5]:

$$\varepsilon_k = \frac{\dot{E}x_{P,k}}{\dot{E}x_{F,k}} \quad (4)$$

Table 1 illustrates the exergy destruction rate and efficiency relations for each component of the desired system.

Table 1. Exergy destruction rates and exergy efficiency equations for the system components

Component	Exergy destruction rate definition	Exergy efficiency definition
Turbine	$\dot{E}x_{d,Turbine} = \dot{E}x_5 - \dot{E}x_6 - \dot{W}_{out,Turbine}$	$\varepsilon_{Turbine} = \frac{\dot{W}_{out,Turbine}}{\dot{E}x_5 - \dot{E}x_6}$
Evaporator	$\dot{E}x_{d,Evaporator} = \dot{E}x_{17} + \dot{E}x_{19} - \dot{E}x_{18} - \dot{E}x_{20}$	$\varepsilon_{Evaporator} = \frac{\dot{E}x_{17} - \dot{E}x_{18}}{\dot{E}x_{19} - \dot{E}x_{20}}$
Heat exchanger 1	$\dot{E}x_{d,HeatExchanger1} = \dot{E}x_2 + \dot{E}x_8 - \dot{E}x_3 - \dot{E}x_5$	$\varepsilon_{HeatExchanger1} = \frac{\dot{E}x_8 - \dot{E}x_5}{\dot{E}x_2 - \dot{E}x_3}$
Condenser	$\dot{E}x_{d,Condenser} = \dot{E}x_6 + \dot{E}x_9 - \dot{E}x_{10} - \dot{E}x_7$	$\varepsilon_{Condenser} = \frac{\dot{E}x_9 - \dot{E}x_{10}}{\dot{E}x_6 - \dot{E}x_7}$
Heat exchanger 2	$\dot{E}x_{d,HeatExchanger2} = \dot{E}x_{16} + \dot{E}x_{25} - \dot{E}x_{15} - \dot{E}x_{26}$	$\varepsilon_{HeatExchanger2} = \frac{\dot{E}x_{25} - \dot{E}x_{26}}{\dot{E}x_{16} - \dot{E}x_{15}}$
Heat exchanger 3	$\dot{E}x_{d,HeatExchanger3} = \dot{E}x_{22} + \dot{E}x_{24} - \dot{E}x_{23} - \dot{E}x_{25}$	$\varepsilon_{HeatExchanger3} = \frac{\dot{E}x_{24} - \dot{E}x_{25}}{\dot{E}x_{22} - \dot{E}x_{23}}$
Pump 1	$\dot{E}x_{d,Pump1} = \dot{E}x_1 - \dot{E}x_2 + \dot{W}_{in,Pump1}$	$\varepsilon_{Pump1} = \frac{\dot{E}x_1 - \dot{E}x_2}{\dot{W}_{in,Pump1}}$
Pump 2	$\dot{E}x_{d,Pump2} = \dot{E}x_7 - \dot{E}x_8 + \dot{W}_{in,Pump2}$	$\varepsilon_{Pump2} = \frac{\dot{E}x_7 - \dot{E}x_8}{\dot{W}_{in,Pump2}}$
Pump 3	$\dot{E}x_{d,Pump3} = \dot{E}x_{21} - \dot{E}x_{22} + \dot{W}_{in,Pump3}$	$\varepsilon_{Pump3} = \frac{\dot{E}x_{21} - \dot{E}x_{22}}{\dot{W}_{in,Pump3}}$
CPV/T based electrolysis	$\dot{E}x_{d,Electrolyzer} = \dot{E}x_{11} - \dot{E}x_{12} - \dot{E}x_{13} + \dot{W}_{Electrolyzer}$	$\varepsilon_{Electrolyzer} = \frac{\dot{E}x_{12} + \dot{E}x_{13}}{\dot{W}_{Electrolyzer}}$
Heater Magnetocaloric beds	$\dot{E}x_{d,HeaterMG} = \dot{E}x_{20} - \dot{E}x_{21} + \dot{W}_{Heating}$	$\varepsilon_{HeaterMG} = \frac{\dot{E}x_{20} - \dot{E}x_{21}}{\dot{W}_{Heating}}$
Cooler Magnetocaloric beds	$\dot{E}x_{d,CoolerMG} = \dot{E}x_{23} - \dot{E}x_{19} + \dot{W}_{Cooling}$	$\varepsilon_{CoolerMG} = \frac{\dot{E}x_{23} - \dot{E}x_{19}}{\dot{W}_{Cooling}}$
Solar CPV/T	$\dot{E}x_{d,CPV} = \dot{E}x_{15} - \dot{E}x_{16} - \dot{W}_{CPV} + \dot{Q}_{in,solar}(1 - \frac{T_0}{T_{sun}})$	$\varepsilon_{CPV} = \frac{\dot{W}_{CPV} + \dot{E}x_{16} - \dot{E}x_{15}}{\dot{Q}_{in,solar}(1 - \frac{T_0}{T_{sun}})}$

Dryer	$\dot{E}x_{d,Dryer} = \dot{E}x_{26} + \dot{E}x_{28} - \dot{E}x_{27} - \dot{E}x_{29}$	$\varepsilon_{Dryer} = \frac{\dot{E}x_{28} - \dot{E}x_{29}}{\dot{E}x_{26} - \dot{E}x_{27}}$

2.4. PEM electrolyzer simulation

The performance of PEM electrolyzer cells can be expressed by the voltage and current density relationship. The present model assumes that: (a) the catalyst layer is infinitely thin and the electrochemical reaction only occurs at the interface of gas diffusion layer and PEM; (b) gases transferred inside the electrode and channel are ideal gases; (c) the porous electrode means and together and its physical parameters refer to those of gas diffusion layer. The potential of a single PEM electrolyzer cell is composed by the open circuit voltage, activation overpotential, diffusion overpotential, and ohmic loss overpotential. The total relationship is [13]:

$$V = V_{ocv} + V_{act} + V_{diff} + V_{ohm} \quad (5)$$

where V_{ocv} is the open circuit voltage as well as the theoretical minimum voltage for PEM electrolyzer cells when neglecting other overpotentials, V_{act} is the overpotential due to the electrochemical reaction, Vdiff is the diffusion overpotential (concentration overptential) caused by the mass transport in the electrolyzers, and Vohm is the ohmic overpotential caused by the electrolyzer cell resistances. The concentration overpotentials are assumed to be negligible. This is valid if the current density is not too high (i.e. J < 10,000 A/m^2) [14]:

$$V_{ocv} = V_0 + \frac{RT}{zF}\ln\left(\frac{\alpha_{H_2}\alpha_{O_2}^{0.5}}{\alpha_{H_2O}}\right) \quad (6)$$

$$V_0 = 1.229 - 0.9\times10^{-3}(T_{PEM} - 298) \quad (7)$$

The activation overpotential is a potential loss from the electrolysis electrochemical reaction, which can be significantly affected by physical and chemical parameters, such as operating temperat., catalyst property, active reaction site, and electrode morphology. Since some effects are very difficult to model, the activation overpotential in the present model will be typically derived from the Butlere Volmer equation, which is the fundamental electrochemical relationship describing how current depends on the voltage in the electrode.

$$V_{act} = V_{act,a} + V_{act,c} \quad (8)$$

$$V_{act,a} = \frac{RT_a}{\alpha_a F}\sinh^{-1}\left(\frac{J}{2J_{0,a}}\right) = \frac{RT_a}{\alpha_a F}\ln\left(\frac{J}{2J_{0,a}} + \sqrt{1+\left(\frac{J}{2J_{0,a}}\right)^2}\right) \quad (9)$$

$$V_{act,c} = \frac{RT_c}{\alpha_c F}\sinh^{-1}\left(\frac{J}{2J_{0,c}}\right) = \frac{RT_c}{\alpha_c F}\ln\left(\frac{J}{2J_{0,c}} + \sqrt{1+\left(\frac{J}{2J_{0,c}}\right)^2}\right) \quad (10)$$

where $V_{act,a}$ and $V_{act,c}$ are the anode and cathode voltage respectively, T_a and T_c indicate the anode and cathode operating temperat. respectively, which are equal to electrolyzer operating temperat. in the present model, and aa and ac are the charge transfer coefficient at the anode and cathode. α_a =2.0 and αc = 0.5 are typically values for PEM electrolyzer cells . j is the current density on the electrodes. $j_{0,a}$ and $j_{0,c}$ are the exchange current density on the anode and cathode electrode, which also vary greatly according to different papers and play an important role in PEM electrolyzer cell modeling. Ohmic overpotential across the proton exchange membrane is caused by the resistance of the membrane to the hydrogen ions transporting through it. The ionic resistance of the membrane is related to the degree of humidification and thickness of the membrane as well as the membrane temperat.. The local ionic conductivity σ(x) of the membrane has been empirically determined as [14]:

$$\sigma_{PEM}[\lambda(x)] = [0.5139\lambda(x) - 0.326]\exp[1268(\frac{1}{303} - \frac{1}{T})] \quad (11)$$

where x is the depth in the membrane meas.d from the cathode membrane interface; λ(x) is the water content at location x in the membrane. The value of λ(x) can be determined in terms of water content at the membrane-electrode interfaces.

$$\lambda(x) = \frac{\lambda_a - \lambda_c}{L}x + \lambda_c \quad (12)$$

where L is the membrane thickness; λ_a and λ_c are the water contents at the anode-membrane and the cathode-membrane interface, respectively. The overall ohmic resistance (RPEM) can thus be determined as:

$$R_{PEM} = \int_0^L \frac{dx}{\sigma_{PEM}[\lambda(x)]} \quad (13)$$

The ohmic overpotential can be expressed in terms of ohm's law:

$$V_{ohm,PEM} = JR_{PEM} \quad (14)$$

The energy and exergy efficiency of PEM electrolyzer can be calculated using following relations [15]:

$$\eta_{en} = \frac{LHV_{H_2}\times\dot{N}_{H_2,out}}{Q_{electric} + Q_{heat,PEM}} \quad (15)$$

$$\eta_{ex} = \frac{Ex_{H_2}\times\dot{N}_{H_2,out}}{Ex_{electric} + Ex_{heat,PEM}} \quad (16)$$

2.5.Exergoeconomic balance

To calculate the cost of exergy destruction rate in each component, the cost balance should be used as [5]:

$$\sum_{out} c\dot{E}x = \sum_{in} c\dot{E}x + \dot{Z} \quad (17)$$

In Eq. (17), c refers to the cost per unit exergy and $\dot{Z}$ indicates the investment and maintenance cost rate. The cost balance and the auxiliary equation based on the fuel and product rules are listed in Table 2.

The major parameters to assess the cost performance of the system are presented as follows:

Exergy destruction cost rate within the kth component, $\dot{C}_{D,k}$:

$$\dot{C}_{D,k} = c_{F,k}\dot{E}x_{D,k} \quad (18)$$

In Eq. (18), cF represents the cost per exergy of fuel.

- Exergoeconomic factor, f_c :

$$f_{c,k} = \frac{\dot{Z}_k}{\dot{Z}_k + \dot{C}_{D,k}} \quad (19)$$

- Relative cost difference, representing the potential of cost reduction within the kth component, r_c:

$$r_{c,k} = \frac{c_{P,k} - c_{F,k}}{c_{F,k}} \quad (20)$$

Table 2. Cost balance and auxiliary relations for each component

Item	Cost balance	Auxiliary equation
Pump 1 and well	$c_{Pump1}\dot{W}_{Pump1} + \dot{Z}_{pump1} + \dot{Z}_{geo} = c_2\dot{E}x_2$	$c_{Pump1} = c_{turbine}$
Heat exchanger 1	$c_2\dot{E}x_2 + c_8\dot{E}x_8 + \dot{Z}_{HeatExchanger1} = c_3\dot{E}x_3 + c_5\dot{E}x_5$	$c_2 = c_3$
Turbine	$c_5\dot{E}x_5 + \dot{Z}_{turbine} = c_6\dot{E}x_6 + c_{turbine}\dot{W}_{turbine}$	$c_5 = c_6$
pump 2	$c_7\dot{E}x_7 + c_{Pump2}\dot{W}_{Pump2} + \dot{Z}_{pump2} = c_8\dot{E}x_8$	$c_{Pump2} = c_{turbine}$
Condenser	$c_6\dot{E}x_6 + c_9\dot{E}x_9 + \dot{Z}_{Condenser} = c_7\dot{E}x_7 + c_{10}\dot{E}x_{10}$	$c_6 = c_7$
PEM electrolyzer	$c_{11}\dot{E}x_{11} + c_{electrolyzer}\dot{W}_{electrolyzer} + \dot{Z}_{electrolyzer} = c_{13}\dot{E}x_{13} + c_{12}\dot{E}x_{12}$	$c_{13} = c_{12}$
CPVT	$\dot{C}_{sun} + c_{15}\dot{E}x_{15} + \dot{Z}_{CPV/T} = c_{16}\dot{E}x_{16} + c_{electrolyzer}\dot{W}_{electrolyzer}$	$\dot{C}_{sun} = 0$ $c_{electrolyzer} = \frac{c_{16}\dot{E}x_{16} - c_{15}\dot{E}x_{15}}{\dot{E}x_{16} - \dot{E}x_{15}}$
Heat exchanger 2	$c_{16}\dot{E}x_{16} + c_{25}\dot{E}x_{25} + \dot{Z}_{HeatExchanger2} = c_{15}\dot{E}x_{15} + c_{26}\dot{E}x_{26}$	$c_{15} = c_{16}$
Heat exchanger 3	$c_{24}\dot{E}x_{24} + c_{22}\dot{E}x_{22} + \dot{Z}_{HeatExchanger3} = c_{23}\dot{E}x_{23} + c_{25}\dot{E}x_{25}$	$c_{22} = c_{23}$
pump 3	$c_{21}\dot{E}x_{21} + c_{Pump3}\dot{W}_{Pump3} + \dot{Z}_{pump3} = c_{22}\dot{E}x_{22}$	$c_{pump3} = c_{turbine}$
Heater Magnetocaloric beds	$c_{20}\dot{E}x_{20} + c_{MagnetoCaloricBeds}\dot{W}_{heating} + \dot{Z}_{MagnetoCaloricBeds} = c_{21}\dot{E}x_{21}$	$c_{MagnetoCaloricBeds} = c_{electrolyzer}$
Cooler Magnetocaloric beds	$c_{23}\dot{E}x_{23} + c_{MagnetoCaloricBeds}\dot{W}_{cooling} + \dot{Z}_{MagnetoCaloricBeds} = c_{19}\dot{E}x_{19}$	$c_{MagnetoCaloricBeds} = c_{electrolyzer}$
Evaporator	$c_{19}\dot{E}x_{19} + c_{17}\dot{E}x_{17} + \dot{Z}_{evaporator} = c_{20}\dot{E}x_{20} + c_{18}\dot{E}x_{18}$	$c_{19} = c_{20}$
Drier	$c_{26}\dot{E}x_{26} + c_{28}\dot{E}x_{28} + \dot{Z}_{dryer} = c_{27}\dot{E}x_{27} + c_{29}\dot{E}x_{29}$	$c_{26} = c_{27}$

2.5. Exergoenvironmental balance

The exergoenvironmental analysis assigns the environmental impact, obtained from life cycle assessment (LCA), to the exergy streams associated with the components. The environmental balance for the kth component with n inlet and m outlet streams can be formulated by [16]:

$$\sum_{in} b\dot{E}x + \dot{Y} = \sum_{out} b\dot{E}x \quad (21)$$

where b represents the environmental impact per unit of exergy and $\dot{Y}$ is component-related environmental impact rate which can be calculated as [17]. The exergoenvironmental equation of the components are presented in Table 3.

In order to assess the EI of the system several parameters are defined as follows:

- The environmental impact of exergy destruction rate within the k-th component, $\dot{B}_{D,k}$:

$$\dot{B}_{D,k} = b_{F,k}\dot{E}x_{D,k} \quad (22)$$

Here, b_F indicates the environmental impact per exergy of fuel.

- Exergoenvironmental factor within the kth component, $f_{b,k}$:

$$f_{b,k} = \frac{\dot{Y}_k}{\dot{Y}_k + \dot{B}_{D,k}} \quad (23)$$

Relative environmental impact difference, indicating the potential of environmental impact reduction within the kth component, $r_{b,k}$:

$$r_{b,k} = \frac{b_{F,k} - b_{P,k}}{b_{F,k}} \quad (24)$$

In Eq. (24), b_P represents the environmental impact per exergy of product.

Table 3. exergoenvironmental equations

Item	EI equation	Auxiliary equation
Pump 1 and well	$b_{Pump1}\dot{W}_{Pump1} + \dot{Y}_{pump1} + \dot{Y}_{geo} = b_2\dot{E}x_2$	$b_{Pump1} = b_{turbine}$
Heat exchanger 1	$b_2\dot{E}x_2 + b_8\dot{E}x_8 + \dot{Y}_{HeatExchanger1} = b_3\dot{E}x_3 + b_5\dot{E}x_5$	$b_2 = b_3$
Turbine	$b_5\dot{E}x_5 + \dot{Y}_{turbine} = b_6\dot{E}x_6 + b_{turbine}\dot{W}_{turbine}$	$b_5 = b_6$
pump 2	$b_7\dot{E}x_7 + b_{Pump2}\dot{W}_{Pump2} + \dot{Y}_{pump2} = b_8\dot{E}x_8$	$b_{Pump2} = b_{turbine}$
Condenser	$b_6\dot{E}x_6 + b_9\dot{E}x_9 + \dot{Y}_{Condenser} = b_7\dot{E}x_7 + b_{10}\dot{E}x_{10}$	$b_6 = b_7$
PEM electrolyzer	$b_{11}\dot{E}x_{11} + b_{electrolyzer}\dot{W}_{electrolyzer} + \dot{Y}_{electrolyzer} = b_{13}\dot{E}x_{13} + b_{12}\dot{E}x_{12}$	$b_{13} = b_{12}$
CPVT	$\dot{B}_{sun} + b_{15}\dot{E}x_{15} + \dot{Y}_{CPV/T} = b_{16}\dot{E}x_{16} + b_{electrolyzer}\dot{W}_{electrolyzer}$	$\dot{B}_{sun} = 0$ $b_{electrolyzer} = \frac{b_{16}\dot{E}x_{16} - b_{15}\dot{E}x_{15}}{\dot{E}x_{16} - \dot{E}x_{15}}$
Heat exchanger 2	$b_{16}\dot{E}x_{16} + b_{25}\dot{E}x_{25} + \dot{Y}_{HeatExchanger2} = b_{15}\dot{E}x_{15} + b_{26}\dot{E}x_{26}$	$b_{15} = b_{16}$

Heat exchanger 3	$b_{24}\dot{E}x_{24}+b_{22}\dot{E}x_{22}+\dot{Y}_{HeatExchanger3}=b_{23}\dot{E}x_{23}+b_{25}\dot{E}x_{25}$	$b_{22}=b_{23}$
pump 3	$b_{21}\dot{E}x_{21}+b_{Pump3}\dot{W}_{Pump3}+\dot{Y}_{pump3}=b_{22}\dot{E}x_{22}$	$b_{pump3}=b_{turbine}$
Heater Magnetocaloric beds	$b_{20}\dot{E}x_{20}+b_{MagnetoCaloricBeds}\dot{W}_{heating}+\dot{Y}_{MagnetoCaloricBeds}=b_{21}\dot{E}x_{21}$	$b_{MagnetoCaloricBeds}=b_{electrolyzer}$
Cooler Magnetocaloric beds	$b_{23}\dot{E}x_{23}+b_{MagnetoCaloricBeds}\dot{W}_{cooling}+\dot{Y}_{MagnetoCaloricBeds}=b_{19}\dot{E}x_{19}$	$b_{MagnetoCaloricBeds}=b_{electrolyzer}$
Evaporator	$b_{19}\dot{E}x_{19}+b_{17}\dot{E}x_{17}+\dot{Y}_{evaporator}=b_{20}\dot{E}x_{20}+b_{18}\dot{E}x_{18}$	$b_{19}=b_{20}$
Drier	$b_{26}\dot{E}x_{26}+b_{28}\dot{E}x_{28}+\dot{Y}_{dryer}=b_{27}\dot{E}x_{27}+b_{29}\dot{E}x_{29}$	$b_{26}=b_{27}$

2.6. PEM Electrolyzer Validation

Simulation accuracy is performed for PEM electrolyzer. Fig. 2 illustrates the comparison of the results obtained from the simulation of the current PEM electrolyzer with those presented in [18]. Refereeing to Fig. 2, as current density varies from 0 to 5500 A/m^2, the cell potential of present model with those obtained from experimental data show the little NRMSD (normalized root square mean deviation) and RMSD (root square mean deviation) values within 0.205 and 0.038 indicting the good agreement.

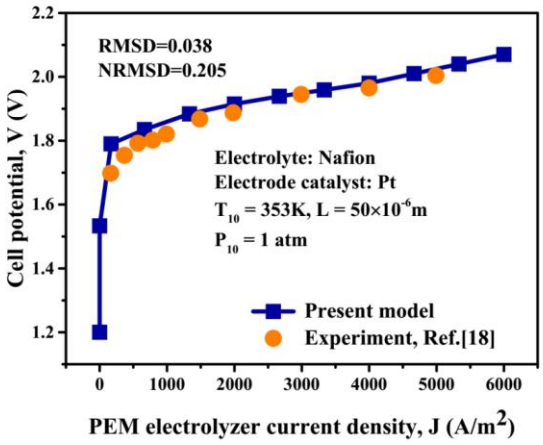

Figure 2. The effects of current density on cell potential

3. Results & Discussion

Table 4 indicates the input parameters used to simulate the desired system and Table 5 lists the outputs calculated. As clearly observed, the energy and exergy efficiencies of PEM electrolyzer to produce H_2 is 61.8% and 58.25%, respectively. Moreover, the product cost and EI rates of H_2 are calculated within 1.268 $/year and 227.6 Pts/year, respectively.

Table 4. input data	
Turbine inlet temperat., T_5 (K)	410
Turbine inlet press., P_5 (kPa)	1500
Isobutane mass flow rate, $\dot{m}_5$ (kg/s)	25
Adiabatic temperat. rise in the magnetic material, ΔC (K)	16
Electrolyzer inlet temperat., T_{10} (K)	343
Current density, J (A/m^2)	3000
Exchange current density(anode), (A/m^2)	0.0001
Exchange current density(cathode), (A/m^2)	0.1

Table 5. performance	
Energetic efficiency of H_2, $\eta_{th,H2}$ (%)	61.8
Exergetic efficiency of H_2, $\eta_{ex,H2}$ (%)	58.25
Net output power, (kw)	838.5
Dry products, (kg/s)	2.072
H_2 production, (kg/day)	2.686
Cooling load, (kw)	11.27
Heating load, (kw)	11577
Cost rate of H_2 production, $\dot{C}_{H_2}$ ($/year)	1.268
Environmental impact rate of H_2 production, $\dot{B}_{H_2}$ (Pts/year)	227.6

Table 6 implies the exergy, economic and EI analyses. Outcomes indicate that the maximum exergy destruction rate is related to heat exchanger 1 followed by the condenser and turbine within 44.7%, 25.94% and 12.46% of the total exergy destruction rate, respectively. The high value of exergy destruction inside heat exchanger 1 is due to the great value of mass flow rate exiting the geothermal well.

The economic analysis shows that the highest investment cost is due to heat exchanger 1 within 34.17% of total investment cost rate and turbine is in the next ranking with value of 30.23%. According to Table 4, the total cost rates ($\dot{Z}+\dot{C}$) dominate in heat exchangers 1 and 2. In turbine, 67.76% of total cost rate belongs to the investment cost rate so that reducing the investment cost rate can increase f up to the desirable value. The value of 100% for the exergoeconomic factor of well and CPVT indicate zero values for costs of exergy destruction rates and all costs are owing to the investment ones. Indeed, all values of f are due to the investment cost rates. The infinite value of the relative cost difference (r) is due to zero value of fuel cost. The lowest value of f is related to the cooler magnetocalric bed meaning that their costs belong to the high value of the exergy destruction rates. Since the beds investment costs are function of mass, reducing their mass can lessen f inside the magnetic refrigeration subsystem. Referring to results obtained from the exergoenvironmental analysis, it is

concluded that EIs of heat exchangers 1 and 2, PEM electrolyzer and the turbine dominant. Additionally, the component-related EI in the most of components are higher than the EI rates associated with the exergy destruction rate. Therefore, to reduce the EI, focus should be put on The EIs of PEM electrolyzer as well as magnetic beds. Due to zero values of fuels, EIs associated with exergy destruction rate for solar and geothermal energies are zero. In PEM electrolyzer, heat exchangers 1 and 2, f_b is higher than 50%. In other components, EIs due to the exergy destruction are more effective.

Table 6. Results obtained from the exergy, exergoeconomic and exergoenvironmental analyses

Components	Exergetic analysis		Exergoeconomic analyses							Exergoenvironmental analysis				
	$\dot{E}x_D$ (kW)	ε (%)	Z ($)	$\dot{Z}$ ($/year)	c_F ($/GJ)	$\dot{C}_D$ ($/year)	$\dot{Z}+\dot{C}_D$ ($/year)	r_c (-)	f_c (%)	$\dot{Y}$ (Pts/year)	$\dot{B}_D$ (Pts/year)	$\dot{Y}_D+\dot{B}_D$ (Pts/year)	r_b (-)	f_b (%)
Turbine	187.20	81.75	785104	9488	0.76	4514	14002	0.71	67.76	27.68	38.02	65.70	0.40	42.13
Evaporator	0.21	49.38	8155	98.55	484.80	3143	3241.55	1.06	3.04	0.40	84.97	85.37	1.03	0.47
Heat exchanger 1	671.50	78.00	887381	10724	0.15	3198	13922	1.26	77.03	119.54	18.97	138.51	2.11	86.30
Condenser	389.70	73.64	563682	6812	0.38	4690	11502	0.93	59.22	64.75	39.50	104.25	0.99	62.11
Heat exchanger 2	6.23	63.61	23685	286.20	2.29	450	736.20	0.95	38.87	0.62	9.11	9.73	0.62	6.37
Heat exchanger 3	1.36	39.42	20099	242.90	91.77	3945	4187.90	1.63	5.80	0.51	105.21	105.72	1.54	0.48
Pump 1	0.27	96.45	8600	103.90	13	111.60	215.50	0.08	48.21	0.06	0.16	0.22	0.06	27.27
Pump 2	100.80	48.91	34373	415.40	1.82	5769	6184.40	1.17	6.72	0.06	42.11	42.17	1.09	0.14
Pump 3	3.37	28.56	7470	90.28	43.60	4628	4718.28	2.63	1.91	0.06	125.11	125.17	2.58	0.05
CPV/T based electrolysis	2.28	60.77	3440	41.57	0.59	42.25	83.82	1.33	49.59	44.15	0.79	44.94	38.04	98.24
Heater Magnetocaloric beds	20.83	6.22	1101	13.30	9.02	5923	5936.30	15.12	0.22	3.15	159.42	162.57	15.38	1.94
Cooler Magnetocaloric beds	20.97	5.91	1101	13.30	9.38	6204	6217.30	14.79	0.21	3.15	164.93	168.08	15.06	1.88
Geothermal well	-	-	212371	2567	0	0	2567	infinity	100	3.15	0	3.15	infinity	100
Solar CPV/T	91.83	25.54	33926	410	0	0	410	infinity	100	9.46	0	9.46	infinity	100
Dryer	5.60	42.72	6433	77.74	4.31	761.10	838.84	1.49	9.27	0.61	12.13	12.74	1.42	4.79

3.1. Parametric Assessment

Fig. 3 illustrates the turbine inlet temperat. and (T_5) and press. (P_5) on the exergetic and product cost rate of PEM electrolyzer. Results show that the increment of these parameters do not affect the exergetic and cost criteria. As T_5 increases, the product cost of H_2 increases within 7%. This trend is due to the increment of product cost of exergy unit in the condenser by 35% leading to the increasing of the required fuel cost of PEM electrolyzer. As press. lines indicate, the increase of P_5, the cost of H_2 production decreases within 28% because the operation of the turbine is improved and the product cost of exergy unit of the heating load lowers within 23%.

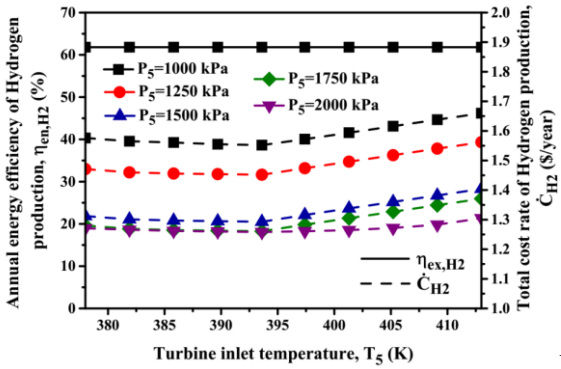

Figure 3. The effects of turbine inlet temperature and press. on the PEM electrolyzer efficiency and cost

The behavior of the environmental impact of H_2 with changes of T_5 and P_5 is illustrated in Fig. 4.

According to the results , T_5 has a slight negative effect on the environmental impact of H_2 within 0.13% because with growth of the heating load exergy within 21%, its EI increases 52%. On the other hand, when P_5 grows, EI associated with H_2 production increases 0.09%. Moreover, the improved operation of the turbine, the exergy and EI of the heating load reduce about 26.6%.

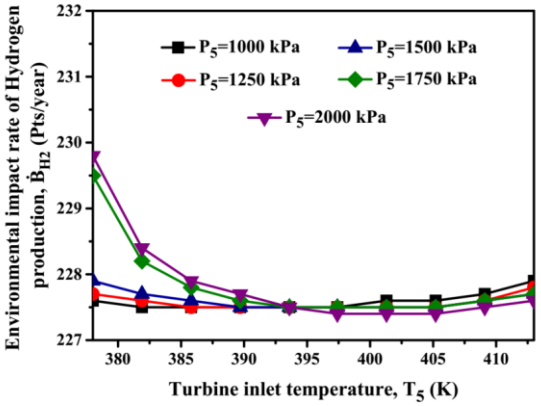

Figure 4. The effects of turbine inlet temperature and press. on the PEM electrolyzer EI

The impacts of PEM electrolyzer current density (J) as well as temperature. (T_{10}) on exergetic efficiency and cost of H_2 production are shown in Fig. 5. Increasing of J causes the reduction of the exergetic efficiency of H_2 within 4.26% due to the increase of PEM electrolyzer inlet electricity (about 2 times). Moreover, T_{10} has a positive effect on the exergetic efficiency of the H_2 production within 1.82% due to the improvement of PEM electrolyzer operation and reduction of the consumed electricity. Outcomes indicate that the growth of J increases the cost of H_2 production up to 3.6 times because J causes the increase of the inlet power as well as the CPVT area consequently the power cost produced is increased. As T_{10} increases, the cost of H_2 increases (about 15.7%) and PEM electrolyzer operation is improved leading to the decrement of the investment cost of CPVT and PEM electrolyzer within 2.68% and 2.69%, respectively. On the other hand, T_{10} growth and consequently the increase of H_2 temperat. causes the cost of this product within 12.37%.

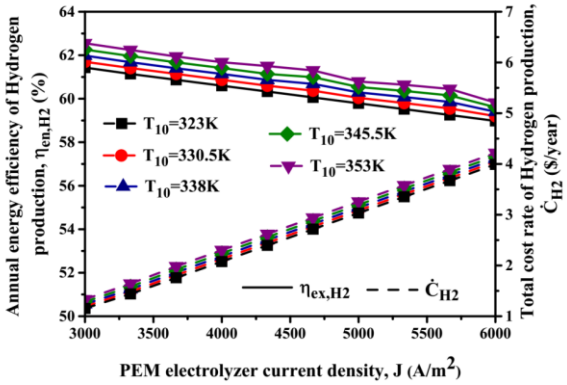

Figure 5. The effects of PEM electrolyzer current density and temperature on the PEM electrolyzer efficiency and cost

Fig. 6 illustrates the effects of J and T_{10} on the EI of H_2 production. As J increases when remaining parameters are kept constant, the EI of H_2 production gets 2 times due to the increase of its exergy. Moreover, the growth of T_{10} has a little impact on the EI of H_2 (about 0.22) due to the increase of the H_2 exergy (2.01 times).

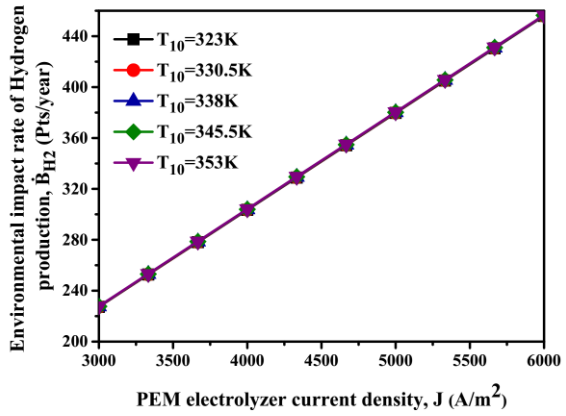

Figure 6. The effects of PEM electrolyzer current density and temperature on the PEM electrolyzer EI

Fig. 7 demonstrates the impacts of the ORC mass flow rate ($\dot{m}_5$) and adiabatic temperat. difference of magnetic refrigeration (ΔC) on the exergetic efficiency and cost of H_2. As clearly observed do not affect the exergy and cost. With increase of $\dot{m}_5$, the cost rate of H_2 rises within 3.86% because the product cost of exergy unit for heating load gets 4.1 times. According to results, ΔC has a positive effect on the cost about 32.86% because J remains constant and CPVT area increases leading to reduction of the PEM outputs unit cost about 38%.

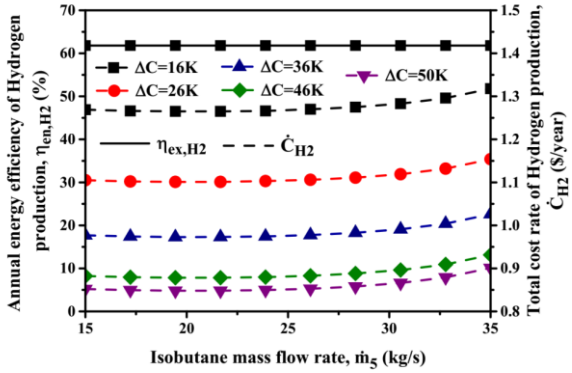

Figure 7. The effects of ORC mass flow rate and adiabatic temperature difference on the energetic efficiency and cost of H_2

The EI behavior of H_2 production with variation of $\dot{m}_5$ and ΔC is illustrated in Fig. 8. As observed, $\dot{m}_5$ has a slight negative effect on EI (0.4%) due to the drastic increase of the heating load EI (6.29 times) while the variation of ΔC has a positive effect on the EI of H_2 (about 2.6 times) because with increase of ΔC, J remains fixed and CPVT area increases causing the reduction of EI of PEM outputs by about 2.7%.

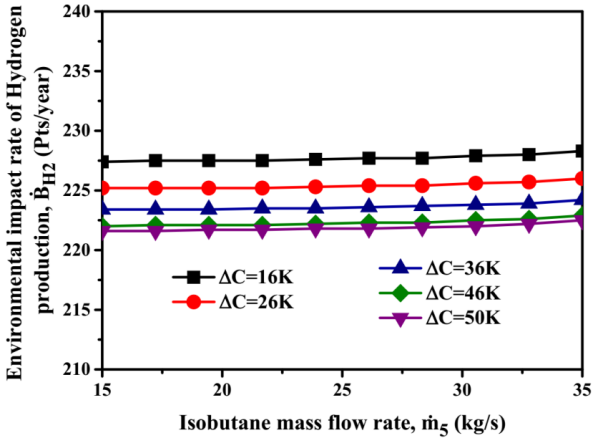

Figure 8. The effects of The effects of ORC mass flow rate and adiabatic temperature difference on the EI of H_2

Fig. 9 shows the impacts of the current density exchanged inside the anode and cathode ($J_{o,a}$ and $J_{o,c}$) on the exergetic efficiency and cost of H_2. It is observed that $J_{o,a}$

and $J_{o,c}$ increments causes the positive effects on the exergetic efficiency and cost within 7.1% and 15.24%, respectively. It is proved that the exchange current density increment improves the operation of the PEM electrolyzer. Moreover, when $J_{o,a}$ and $J_{o,c}$ increase, the cost of H_2 is reduced within 6.47% and 12.78%, respectively because the consumed electricity by PEM reduces leading to the decrement of H_2 cost.

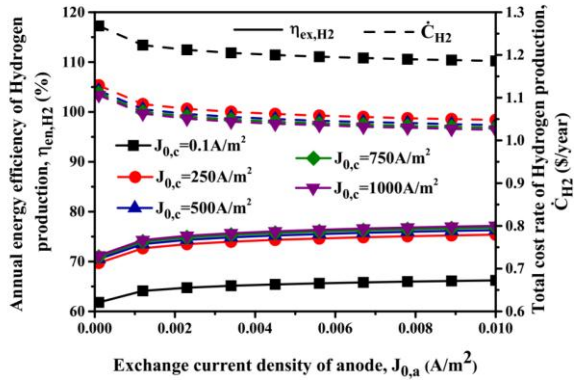

Figure 9. The effects of anode and cathode exchange current densities on energy efficiency and cost of H_2

Fig. 10 shows the behavior of the EI of H_2 versus the anode and cathode exchange current densities on the EI of H_2. Outcomes indicate that $J_{o,a}$ and $J_{o,c}$ increments have the positive impacts on EI within 0.09% and 0.018%, respectively because the total voltage exchanged within PEM reduces meaning the lower consumed electricity. Therefore, the EI of H_2 produced lowers.

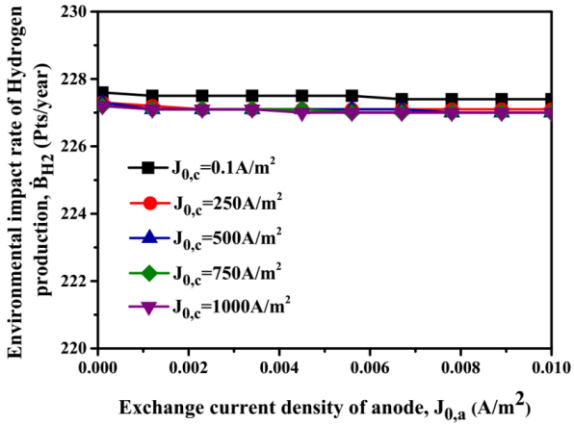

Figure 10. The effects of anode and cathode exchange current densities on the EI of H_2

4. Conclusions

H2 production in PEM electrolyzer in solar-geothermal based multi-generation system are investigated in this communication. The major parameters impacts are evaluated to find the higher efficiencies and lower cost and EI for H2. The main results from this investigation are listed as follows:

1. The energetic and exergetic efficiency of H2 produced are calculated within 61.8% and 58.25%, respectively.
2. The cost and EI of H2 are 1.268 $/year and 227.6 Pts/year, respectively.
3. The maximum exergy destruction, cost and EI belong to heat exchanger 1.
4. All parameters increments have a positive effect on the exergetic efficiency.
5. Increasing the turbine press. reduces the EI rate of H2 within 3.8%.

References

[1] Laboratory, L.A.N., Hydrogen. 5 February 2008: Chemistry Operations (15 December 2003).

[2] Durgutlu, A., Experimental investigation of the effect of hydrogen in argon as a shielding gas on TIG welding of austenitic stainless steel. Materials & design, 2004. 25(1): p. 19-23.

[3] Almqvist, E., History of industrial gases. 2003: Springer Science & Business Media.

[4] Block, M. Hydrogen as tracer gas for leak testing. in Proceedings of the 9th European Conference on Nondestructive Testing (ECNDT): Sept. 25-29, 2006; Berlin. p. Tu. 2.6. 2006.

[5] Ahmadi, P., I. Dincer, and M.A. Rosen, Energy and exergy analyses of hydrogen production via solar-boosted ocean thermal energy conversion and PEM electrolysis. International Journal of Hydrogen Energy, 2013. 38(4): p. 1795-1805.

[6] Ozturk, M. and I. Dincer, Thermodynamic analysis of a solar-based multi-generation system with hydrogen production. Applied Thermal Engineering, 2013. 51(1): p. 1235-1244.

[7] Ahmadi, P., I. Dincer, and M.A. Rosen, Development and assessment of an integrated biomass-based multi-generation energy system. Energy, 2013. 56: p. 155-166.

[8] Ahmadi, P., I. Dincer, and M.A. Rosen, Thermodynamic modeling and multi-objective evolutionary-based optimization of a new multigeneration energy system. Energy Conversion and Management, 2013. 76: p. 282-300.

[9] Ahmadi, P., I. Dincer, and M.A. Rosen, Multi-objective optimization of a novel solar-based multigeneration energy system. Solar Energy, 2014. 108: p. 576-591.

[10] Bicer, Y. and I. Dincer, Development of a new solar and geothermal based combined system for hydrogen production. Solar Energy, 2016. 127: p. 269-284.
[11] Gabbrielli, R., A novel design approach for small scale low enthalpy binary geothermal power plants. Energy Conversion and Management, 2012. 64: p. 263-272.
[12] Bejan, A. and G. Tsatsaronis, Thermal design and optimization. 1996: John Wiley & Sons.
[13] Han, B., et al., Electrochemical performance modeling of a proton exchange membrane electrolyzer cell for hydrogen energy. International Journal of Hydrogen Energy, 2015. 40(22): p. 7006-7016.
[14] Ni, M., M.K. Leung, and D.Y. Leung, Energy and exergy analysis of hydrogen production by a proton exchange membrane (PEM) electrolyzer plant. Energy conversion and management, 2008. 49(10): p. 2748-2756.
[15] Esmaili, P., I. Dincer, and G. Naterer, Energy and exergy analyses of electrolytic hydrogen production with molybdenum-oxo catalysts. International Journal of Hydrogen Energy, 2012. 37(9): p. 7365-7372.
[16] Meyer, L., et al., Exergoenvironmental analysis for evaluation of the environmental impact of energy conversion systems. Energy, 2009. 34(1): p. 75-89.
[17] Manesh, M.K., et al., New proced. for optimal design and evaluation of cogeneration system based on advanced exergoeconomic and exergoenvironmental analyses. Energy, 2013. 59: p. 314-333. 18.